Kestin et al.[6] than the GHS model. This suggests that the assumption of a finite collision probability at $g = 0$ is more realistic than the infinite value given by the GHS model.

The collision frequency of the MGHS model $\nu_{\mathrm{MGHS}} = n\langle \sigma g \rangle$ is given by

$$\nu_{\mathrm{MGHS}} = 4nV_r(\hat{T}/\pi)^{\frac{1}{2}}(C + D) \tag{4}$$

where C and D are similar in form to A and B, respectively, and are given by

$$C(\hat{T}) = \alpha[I_3(0) - I_3(a)] + \hat{T}^{-\frac{1}{2}}(\hat{V}^* - \alpha\hat{g}^*)[I_2(0) - I_2(a)]$$

$$2D(\hat{T}) = \phi\hat{T}^{-\upsilon_1}\Gamma\left(2 - \upsilon_1, a^2\right) + (1 - \phi)\hat{T}^{-\upsilon_2}\Gamma\left(2 - \upsilon_2, a^2\right)$$

From Eqs. (1) and (4), it can be shown that ν_{MGHS} is considerably lower than ν_{GHS} for $\hat{T} \lesssim 1$. For example, at $\hat{T} = (1, 0.5, 0.1, 0.05)$, $\nu_{\mathrm{MGHS}}/\nu_{\mathrm{GHS}} \approx (0.92, 0.83, 0.49, 0.35)$.

Computational Efficiency

The computational efficiency of the GHS and MGHS models under conditions of thermal equilibrium was determined by simulations for a set of 1000 monatomic simulator molecules for a time of $100\tau_{\mathrm{nom}}$, where $\tau_{\mathrm{nom}} = \pi\mu_{\mathrm{GHS}}/(4\rho RT)$. The simulation time step Δt was $0.4\tau_{\mathrm{nom}}$. Temperatures of 100, 300, and 3000 K were simulated. At each time step, the number of collision pairs tested and the actual number of collisions performed were recorded. Simulations were also performed using the VHS model, with $\upsilon = 0.22$ and the viscosity matched to μ_{GHS}. The number of collisions per simulator particle per time τ_{nom} is independent of T for the VHS model, and a single VHS simulation was, therefore, sufficient.

The mean results from the second-half of each simulation are summarized in Table 1. The results are subject to statistical scatter, but demonstrate the poor computational efficiency of the GHS model, even at high temperatures. This inefficiency is caused primarily by the high number of pairs tested at each time step due to very high values of $V_{\max}$, but also by the higher collision frequency. The MGHS model requires no more than 15% more CPU time than the VHS model.

Conclusions

The GHS model can be modified to limit the collision probability at low collision speeds. This improves the computational efficiency both because the number of possible collision partners that must be tested is dramatically reduced and because the collision rate is lower. No more than 15% extra computational time is required, compared with the VHS model. For argon at $T \approx 100$ K, the theoretical viscosity is changed by less than 2.5%, and this difference decreases rapidly as T increases. The modified viscosity is in better agreement with recommended viscosity values. This modified generalized hard sphere model can be used in DSMC simulations, where, to obtain realistic viscosity behavior at low T, it is necessary to model the effect of the attractive portion of the intermolecular potential.

References

[1] Bird, G. A., *Molecular Gas Dynamics and the Direct Simulation of Gas Flows*, Oxford Univ. Press, New York, 1994.

[2] Hassan, H. A., and Hash, D. B., "A Generalized Hard-Sphere Model for Monte Carlo Simulation," *Physics of Fluids A*, Vol. 5, No. 3, 1993, pp. 738–744.

[3] Hash, D. B., Moss, J. N., and Hassan, H. A., "Direct Simulation of Diatomic Gases Using the Generalized Hard Sphere Model," *Journal of Thermophysics and Heat Transfer*, Vol. 8, No. 4, 1994, pp. 758–764.

[4] Kuščer, I., "A Model for Rotational Energy Exchange in Polyatomic Gases," *Physica A*, Vol. 158, 1989, pp. 784–800.

[5] Boyd, I. D., "Temperature Dependence of Rotational Relaxation in Shock Waves of Nitrogen," *Journal of Fluid Mechanics*, Vol. 246, Jan. 1993, pp. 343–360.

[6] Kestin, J., Knierim, K., Mason, E. A., Najafi, B., Ro, S. T., and Waldman, M., "Equilibrium and Transport Properties of the Noble Gases and Their Mixtures at Low Density," *Journal of Physical and Chemical Reference Data*, Vol. 13, No. 1, 1984, pp. 229–303.

Impingement Heat Transfer over a Rotating Disk: Integral Method

I. V. Shevchuk*
Ukrainian National Academy of Sciences, 03057 Kiev, Ukraine
and
N. Saniei† and X. T. Yan‡
Southern Illinois University, Edwardsville, Illinois 62026-1805

Nomenclature

A	=	dimensionless parameter ($= ad_j/V_j$)
a	=	radial velocity gradient at the outer edge of the boundary layer
c_p	=	specific heat at constant pressure
d	=	disk diameter
d_j, h_j	=	jet nozzle diameter and nozzle-to-disk distance
k	=	thermal conductivity
Nu_d	=	local Nusselt number ($= q_w d/[k(T_w - T_\infty)]$)
Pr	=	Prandtl number ($= \mu c_p/k$)
q_w	=	heat flux at the wall
Re_j	=	jet Reynolds number ($= V_j d_j/\nu$)
Re_ω	=	rotational Reynolds number ($= \omega d^2/\nu$)
r, φ, z	=	radial, tangential, and axial cylindrical coordinates
T	=	temperature
V_j	=	axial velocity at infinity or at the nozzle outlet
v_r, v_φ, v_z	=	radial, tangential, and axial velocity components in cylindrical coordinates
δ	=	boundary-layer thickness
δ_T^{**}	=	enthalpy thickness $\left(= \int_0^1 \frac{v_r}{\omega r}\frac{T - T_\infty}{T_w - T_\infty}\,\mathrm{d}\xi\right)$
κ	=	nondimensional parameter ($= a/\omega$)
μ, ν	=	dynamic and kinematic viscosity
ρ	=	density
τ_{wr}	=	radial shear stress $[= \mu(\mathrm{d}v_r/\mathrm{d}z)_{z=0}]$
$\tau_{w\varphi}$	=	tangential shear stress $[= \mu(\mathrm{d}v_\varphi/\mathrm{d}z)_{z=0}]$
χ	=	Reynolds analogy parameter $\{= q_w\omega r/[\tau_{w\varphi}c_p(T_\infty - T_w)]\}$
ω	=	angular speed of rotation

Subscripts

j	=	parameters of the impinging jet
w	=	wall
0	=	free disk
∞	=	outer edge of the boundary layer

Introduction

UNDERSTANDING of peculiarities of real jets is frequently based on the solutions of simplified problems. For an

Received 30 August 2002; revision received 4 December 2002; accepted for publication 4 December 2002.

*Senior Staff Scientist, Institute of Engineering Thermophysics, 2a, Zhelyabov St.; ivshevch@i.com.ua.

†Professor, Department of Mechanical and Industrial Engineering; nsaniei@siue.edu.

‡Associate Professor, Department of Mechanical and Industrial Engineering; xyan@siue.edu. Member AIAA.

axisymmetric laminar jet impinging on a stationary surface at $\omega = 0$, it was shown[1] that a constant-thickness boundary layer develops near the stagnation point, whereas the velocity components at the outer edge of the boundary layer are described by the equations

$$v_{r,\infty} = ar, \qquad v_{z,\infty} = -2az \tag{1}$$

$$A = 4/\pi \qquad \text{or} \qquad A = 1.5 \cdot (h_j/d_j)^{-0.22} \tag{2}$$

The first of relations (2) is valid for the potential flow of a uniform stream impinging on the disk[1]; in this case $d_j = d$. The second equation (2) is effective for real singular axisymmetric jets[2] over the range $h_j/d_j = 2 \ldots 6$ for high enough values of Re_j, whereas $A \approx 1$ for low values of Re_j.

For coaxial uniform flow impingement on a rotating disk, works[1,3] present velocity profiles and friction coefficients in the graphical or tabulated form. Nusselt numbers were calculated for the boundary condition (here c_0 is constant)

$$T_w - T_\infty = c_0 r^{n^*} \tag{3}$$

only at $n^* = 0$ and 2 for few values of Pr and κ in works.[1,3] Experimental radial distributions of the Nusselt number are presented in papers.[4,5] At $V_j = 0$ the problem reduces to the case of the free rotating disk studied extensively in works.[1,3,6]

The main objective of the present work consists of the development of an integral method and obtaining an approximate analytical solution of the problem under consideration. This method is based on the exact numerical solution of the Navier–Stokes and energy equations under conditions (1) and (3) at 10 values of $n^* = -2 \ldots 4$, different $Pr = 0.1 \ldots 1$ and $\kappa = 0 \ldots \infty$.

Integral Method for Fluid Flow and Heat Transfer

Integral equations of the boundary layer and model for the velocity profiles are

$$\frac{\mathrm{d}}{\mathrm{d}r}\left[r\int_0^\delta v_r(v_{r,\infty} - v_r)\,\mathrm{d}z\right] + \frac{\mathrm{d}v_{r,\infty}}{\mathrm{d}r}\int_0^\delta (v_{r,\infty} - v_r)\,\mathrm{d}z + \int_0^\delta v_\varphi^2\,\mathrm{d}z = \frac{r\tau_{wr}}{\rho} \tag{4}$$

$$\frac{\mathrm{d}}{\mathrm{d}r}\left[r^2\int_0^\delta v_r v_\varphi\,\mathrm{d}z\right] = -\frac{r^2\tau_{w\varphi}}{\rho} \tag{5}$$

$$\frac{\mathrm{d}}{\mathrm{d}r}\left[r^2\delta\bar{\delta}_T^{**}(T_w - T_\infty)\right] = \frac{rq_w}{\rho c_p \omega} \tag{6}$$

$$\frac{v_\varphi}{\omega r} = g, \qquad \frac{v_r}{v_{r,\infty}} = (1 - g^*)\kappa + \frac{(\alpha - \kappa)f}{\alpha_0} \tag{7}$$

Here g, g^*, and f are universal functions of the variable z/δ; g and f are determined at $\kappa = 0$; g^* is found in course of solution; $\alpha_0 = 0.8284$. Given $\alpha = \text{const}$ and $\delta = \text{const}$, we found the solution, which coefficients were obtained via agreement with the exact solution,

$$\alpha = -0.4275\kappa + (2.717\kappa^2 + 0.6863)^{\frac{1}{2}} \tag{8}$$

$$\tau_{w\varphi}/\tau_{w\varphi 0} = \delta_0/\delta = [(\alpha + 1.301\kappa)/\alpha_0]^{\frac{1}{2}} \tag{9}$$

Maximal discrepancy of the integral method's data for α and $\tau_{w\varphi}/\tau_{w\varphi 0}$ with respect to the exact solution does not exceed 1.7% and falls sharply with increasing κ.

Generalizing the solution for the free disk,[6] we developed the following model:

$$\bar{\delta}_T^{**}\Big/0.5338\alpha\delta_0(\omega/\nu)^{\frac{1}{2}} = (1/b_2) - 0.6518\chi Pr^{n_p}(b_1/b_2) + \kappa/\alpha\left(e_1\chi^{-1} + e_2\chi + e_3\right) \tag{10}$$

Constants b_1, b_2, and n_p depend only on Pr (see Ref. 6). It follows from Eqs. (5) and (6)

$$(1/b_2) - 0.6518\chi Pr^{n_p}(b_1/b_2) + \kappa/\alpha\left(e_1\chi^{-1} + e_2\chi + e_3\right) = 0.3482 \cdot \chi[4/(2 + n^*)][1 + 1.301(\kappa/\alpha)] \tag{11}$$

Coefficients e_1, e_2, and e_3 depend only on the Prandtl number. Their values are $e_1 = 0.1426$, 0.1591, 0.1800, 0.2007, 0.2042; $e_2 = -0.7227$, -0.7313, -0.7404, -0.7495, -0.7497; $e_2 = 1.0333, 1.1280, 1.2427, 1.3556, 1.3696$ at $Pr = 1, 0.9, 0.8, 0.72, 0.71$, respectively.

For given values e_1, e_2, and e_3, relation (11) was easily solved analytically as a quadratic equation. Expression for the Nusselt number becomes

$$Nu_d = K_1 \cdot (1 + \kappa^{-1})^{\frac{1}{2}} \cdot Re_j^{\frac{1}{2}} \cdot A^{\frac{1}{2}} \tag{12}$$

$$K_1 = 0.6159\chi(1 + \kappa)^{-\frac{1}{2}}\, Pr \cdot \tau_{w\varphi}/\tau_{w\varphi 0} \tag{13}$$

Table 1 presents values of χ found from Eq. (11) at $Pr = 0.71$. Maximal deviations of χ from exact solution do not exceed 2.4%. Calculations for other values of $Pr = 0.1 \ldots 1$ also confirm this conclusion. At $T_w = \text{const}$ and $\kappa \to \infty$ it was found that $K_{1^*} = K_1 \cdot (1 + \kappa^{-1})^{1/2}$ is equal to $0.763 \cdot Pr^{0.4}$, which agrees with the expression documented elsewhere. It is worth noting that χ is a quite conservative parameter and changes with κ far less significantly than K_1.

Table 1 Values of χ at $Pr = 0.71$ from the exact solution and integral method (bold) at laminar flow

κ	$n^* = -2$	$n^* = -1.5$	$n^* = -1$	$n^* = -0.5$	$n^* = 0$	$n^* = 0.5$	$n^* = 1$	$n^* = 2$	$n^* = 3$	$n^* = 4$
0	0	0.2366	0.4330	0.6001	0.7452	0.8732	0.9876	1.1856	1.3533	1.4990
0.1	**0**	**0.2698**	**0.4727**	**0.6430**	**0.7883**	**0.9137**	**1.0231**	**1.2048**	**1.3495**	**1.4674**
0.2	0	0.2941	0.5085	0.6772	0.8165	0.9355	1.0398	1.2172	1.3658	1.4946
0.2	**0**	**0.2944**	**0.5020**	**0.6728**	**0.8162**	**0.9385**	**1.0440**	**1.2168**	**1.3525**	**1.4618**
0.4	0	0.3212	0.5424	0.7108	0.8470	0.9619	1.0616	1.2297	1.3695	1.4902
0.4	**0**	**0.3207**	**0.5337**	**0.7049**	**0.8461**	**0.9648**	**1.0660**	**1.2293**	**1.3556**	**1.4560**
0.6	0	0.3334	0.5572	0.7253	0.8602	0.9733	1.0710	1.2351	1.3710	1.4880
0.6	**0**	**0.3324**	**0.5479**	**0.7191**	**0.8593**	**0.9764**	**1.0756**	**1.2347**	**1.3569**	**1.4536**
0.8	0	0.3388	0.5641	0.7322	0.8665	0.9787	1.0755	1.2377	1.3717	1.4870
0.8	**0**	**0.3382**	**0.5549**	**0.7262**	**0.8658**	**0.9820**	**1.0803**	**1.2374**	**1.3575**	**1.4524**
1.0	0	0.3418	0.5679	0.7359	0.8698	0.9816	1.0779	1.2390	1.3721	1.4864
1.0	**0**	**0.3414**	**0.5587**	**0.7300**	**0.8694**	**0.9851**	**1.0828**	**1.2388**	**1.3579**	**1.4517**
1.5	0	0.3453	0.5721	0.7400	0.8736	0.9848	1.0805	1.2405	1.3725	1.4857
1.5	**0**	**0.3449**	**0.5630**	**0.7343**	**0.8733**	**0.9885**	**1.0856**	**1.2404**	**1.3583**	**1.4510**
2.0	0	0.3464	0.5736	0.7415	0.8749	0.9860	1.0815	1.2411	1.3726	1.4855
2.0	**0**	**0.3463**	**0.5646**	**0.7359**	**0.8748**	**0.9898**	**1.0867**	**1.2410**	**1.3584**	**1.4508**
5.0	0	0.3479	0.5754	0.7433	0.8765	0.9874	1.0826	1.2417	1.3728	1.4852
5.0	**0**	**0.3478**	**0.5664**	**0.7377**	**0.8765**	**0.9913**	**1.0879**	**1.2417**	**1.3586**	**1.4505**
50	0	0.3481	0.5757	0.7436	0.8768	0.9876	1.0829	1.2418	1.3728	1.4852
50	**0**	**0.3481**	**0.5668**	**0.7381**	**0.8768**	**0.9916**	**1.0882**	**1.2418**	**1.3586**	**1.4504**

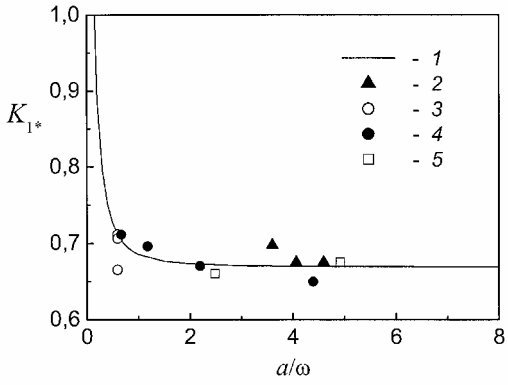

Fig. 1 Effect of parameter κ on the constant K_{1*} at $Pr = 0.71$. 1—present predictions at $T_w = \text{const}$. Experiments[4]: 2—$Re_j = 2.47 \times 10^4$, $Re_d = 8.56 \times 10^5$, $h_j/d_j = 2$, 4, and 6; 3—$Re_j = 6.8 \times 10^3$, $Re_d = 1.584 \times 10^6$, $h_j/d_j = 2$, 4, and 6. Experiments[5]: 4—$Re_j = 6.8 \times 10^3$, $Re_d = 2.14 \times 10^5$, 4.28×10^5, 8×10^5, and 1.412×10^6, $h_j/d_j = 2$; 5—$Re_j = 2.47 \times 10^4$, $Re_d = 8 \times 10^3$, and 1.584×10^6, $h_j/d_j = 2$.

Comparisons with Experiments

For coaxial impingement of jets with $d_j < d$, Eqs. (12) and (13) are valid only inside the stagnation region at $r \le d_j/2$. In this case value d_j is used instead of d in both Nu_d and Re_ω. The disk surface in experiments[4,5] in the stagnation region was practically isothermal ($n^* = 0$). Using the definition of parameter A, we have $\kappa = ARe_j/Re_\omega$. In accordance with Eq. (2), parameter A takes values $A = 1.29$, 1.14, and 1.01 for $h_j/d_j = 2$, 4, and 6, respectively. These values allow reaching good agreement of predictions with experiments[4,5] for Nu_d at $Re_j = 2.47 \times 10^4$. At $Re_j = 6.8 \times 10^3$, experiments do not confirm the tendency of decrease in Nu_d with growing h_j/d_j. The best agreement with experiments at $Re_j = 6.8 \times 10^3$ yields the value $A = 1.12$.

Comparisons of simulations with experiments are shown in Fig. 1. Predictions agree well with experiments clearly exhibiting the tendency of increase with decreasing values of κ. It is apparent also that parameter $K_{1*} = K_1 \cdot (1 + \kappa^{-1})^{1/2}$ is practically constant for $\kappa = 1.5 \ldots \infty$. It means that whenever the parameter κ exceeds the threshold value of 1.5, impingement heat transfer of a rotating disk depends only on Re_j and is independent of the speed of rotation.

Three experimental points fall out of this generally good agreement. Too high experimental value of K_{1*} at $Re_j = 2.47 \times 10^4$, $Re_d = 8.56 \times 10^5$, and $h_j/d_j = 6$ ($\kappa = 3.6$) is probably caused by the too low value $A = 1.01$ used in recalculation of experimental data for Nu_d. Too low experimental value of K_{1*} at $Re_j = 6.8 \times 10^3$, $Re_d = 2.12 \times 10^5$ and $h_j/d_j = 2$ ($\kappa = 4.4$) is probably caused by the fact that we used the constant value $A = 1.12$ in recalculation of Nu_d at $Re_j = 6.8 \times 10^3$ and varying Re_ω, while rotation can affect A at low values of Re_j. Too low value of K_{1*} at $Re_j = 6.8 \times 10^3$, $Re_\omega = 1.584 \times 10^6$, and $h_j/d_j = 4$ ($\kappa = 0.6$) is probably explained by experimental inaccuracy. To clarify the dependence of A on h_j/d_j and Reynolds numbers Re_j and Re_ω, an additional experimental research is needed.

Conclusions

An integral method was developed, and an approximate analytical solution of the problem was derived at $n^* = -2 \ldots 4$. Maximal deviation of the approximate solution from the exact one is 2.4%. At $\kappa > 1.5$ heat transfer is dominated only by peculiarities of the impinging jet. The threshold value of κ is practically independent of Pr and exponent n^*. Present predictions agree well with experiments[4,5] in the vicinity of the stagnation point.

Acknowledgments

These research results were obtained in part as a result of support of the U. S. National Research Council through the Project Development Grant of the Collaboration in Basic Science and Engineering Grants Program. I. V. Shevchuk also acknowledges the support provided by the Research Fellowship of German Academic Exchange Service.

References

[1] Dorfman, L. A., *Hydrodynamic Resistance and the Heat Loss of Rotating Solids*, Oliver and Boyd, Edinburgh, Scotland, U.K., 1963, pp. 9–11.

[2] Brdlik, P. M., and Savin, V. K., "Heat Transfer in the Vicinity of the Stagnation Point at Axisymmetric Jet Flow over Flat Surfaces Located Normally to the Flow," *Journal of Engineering Physics and Thermophysics*, Vol. 10, No. 4, 1966, pp. 423–428.

[3] Tien, C. L., and Tsuji, I. J., "A Theoretical Analysis of Laminar Forced Flow and Heat Transfer About a Rotating Cone," *Journal of Heat Transfer*, Vol. 87, No. 2, 1965, pp. 184–190.

[4] Saniei, N., and Yan, X. T., "An Experimental Study of Heat Transfer from a Disk Rotating in an Infinite Environment Including Heat Transfer Enhancement by Jet Impingement Cooling," *Journal of Enhanced Heat Transfer*, Vol. 7, 2000, pp. 231–245.

[5] Saniei, N., Yan, X. T., and Schooley, W. W., "Local Heat Transfer Characteristics of a Rotating Disk Under Jet Impingement Cooling," *Proceedings of 11th International Heat Transfer Conference*, Vol. 5, Taylor and Francis, Philadelphia, 1998, pp. 445–450.

[6] Shevchuk, I. V., "Effect of the Wall Temperature on Laminar Heat Transfer in a Rotating Disk: An Approximate Analytical Solution," *High Temperature*, Vol. 39, No. 4, 2001, pp. 637–640.

Scale-Size Analysis of Heat and Mass Transfer Correlations

V. Bertola*
Ecole Normale Supérieure, 75005 Paris, France
and
E. Cafaro†
Politecnico di Torino, 10129 Turin, Italy

Nomenclature

C	=	constant coefficient
D	=	characteristic length or hydraulic diameter, m
g	=	gravity acceleration, ms^{-2}
h	=	heat transfer coefficient, $Wm^{-2}K^{-1}$
K	=	transport coefficient, ms^{-1}
k	=	thermal conductivity, $Wm^{-1}K^{-1}$
L	=	macrolength, m
l	=	microlength, m
m	=	convective term exponent
q	=	diffusive term exponent
T	=	macrotime, s
t	=	microtime, s
U	=	mean flow velocity, ms^{-1}
α_M	=	mass diffusivity, m^2s^{-1}
α_T	=	thermal diffusivity, m^2s^{-1}
β	=	expansion coefficient at constant pressure, K^{-1}
ΔT	=	temperature difference, K
η	=	dynamic viscosity, Pa · s
λ	=	macrolength dimensional exponent

Received 10 April 2002; revision received 19 September 2002; accepted for publication 4 December 2002.

*Research Associate, Laboratoire de Physique Statistique, 24 Rue Lhomond. Member AIAA.

†Associate Professor, Dipartimento di Energetica, Corso Duca degli Abruzzi 24.